Elastic and Large-Strain Nonlinear Seismic Site Response from Analysis of Vertical Array Recordings

Eric Yee, M.ASCE[1]; Jonathan P. Stewart, F.ASCE[2]; and Kohji Tokimatsu, M.ASCE[3]

Abstract: Strong ground motions from the $M_w = 6.6$ 2007 Niigata-ken Chuetsu-oki earthquake were recorded by a free-field downhole array at a nuclear power plant. Site conditions consist of about 70 m of medium-dense sands overlying clayey bedrock, with groundwater located at 45 m. Ground shaking at the bedrock level had a geometric mean peak acceleration of 0.55g, which reduced to 0.4g at the ground surface, indicating nonlinear site response. One-dimensional ground response analysis of relatively weak motion aftershock data provides good matches of the observed resonant site frequencies and amplification levels, provided small-strain damping levels somewhat larger than those from laboratory tests are applied. Nonlinear ground response analyses of strong-motion data using laboratory-based modulus reduction and damping relations valid up to moderate strain levels ($< \sim 0.5\%$) produce unrealistic strain localization at a velocity contrast. A procedure is presented to more realistically represent the large-strain portion of backbone curves by asymptotically approaching the shear strength at large strains, which removes strain localization for this application and provides reasonable matches of observed and computed ground motions. **DOI: 10.1061/(ASCE)GT.1943-5606.0000900.** *© 2013 American Society of Civil Engineers.*

CE Database subject headings: Soil dynamics; Earthquakes; Ground motion; Elasticity; Seismic effects; Japan.

Author keywords: Soil dynamics; Site response; Earthquake ground motions.

Introduction

The 2007 $M_w = 6.6$ Niigata-ken Chuetsu-oki earthquake in western Japan caused strong ground shaking at the Kashiwazaki-Kariwa Nuclear Power Plant (KKNPP). As shown in Fig. 1, the KKNPP is located on the hanging wall of the fault above a region of relatively high slip. The focus of this paper is on nonlinear (NL) site response observed in vertical array recordings at the KKNPP site.

Fig. 2 shows a map of the KKNPP including its seven generators (marked as Units 1–7) and three free-field downhole seismic arrays near Units 1 and 5 and the Service Hall. Recordings from the Unit 1 and 5 downhole arrays were overwritten with aftershock data, and only peak accelerations remain. Accordingly, the only recordings utilized are from the Service Hall array (SHA). As shown in Fig. 3, this array contains four three-component accelerometers at depths of 2.4 (Holocene dune sand), 50.8 (Pleistocene Banjin formation), 99.4 (Pliocene Nishiyama formation), and 250 m (Pliocene Nishiyama formation) (Tokimatsu and Arai 2008). (Note that the geotechnical conditions shown in Fig. 3 are described subsequently in the paper.) Groundwater occurs at relatively large depth at the SHA site, so liquefaction effects are neither observed nor are they anticipated from standard triggering techniques [details in Yee et al. (2011)].

Despite the lack of liquefaction, there is evidence for NL soil response at the KKNPP site both from available recordings and from observed ground deformations. As shown in Fig. 2, the recordings indicate deamplification of soil motions relative to rock motions (from the Nishiyama formation) for two of the three arrays (Unit 1 and SHA). The Unit 5 array indicates base-to-surface amplification, but this array is entirely in rock. Ground deformations were observed by Sakai et al. (2009) and Tokimatsu (2008), who observed widespread settlement both in free-field areas and adjacent to reactor structures. Near the SHA site, settlements were approximately 15 ± 5 cm (Yee et al. 2011).

The data set from the SHA site at KKNPP is uniquely valuable. Prior to the 2011 Tohoku Japan earthquake, the SHA recorded the strongest motions for a multidepth vertical array in soil having detailed site characterization. Vertical array recordings enable validation of ground response analysis codes and studies of dynamic soil behavior under in situ conditions (Zeghal et al. 1995; Cubrinovski et al. 1996; Kwok et al. 2008; Tsai and Hashash 2009). With the exception of a few arrays in liquefiable materials, previous vertical array data have generally been at low to modest shaking levels that would not be expected to induce large shear strains associated with strongly NL soil behavior. It is the NL condition where the need for code validation is greatest, and the strong ground motions at SHA are known to have produced NL site response. The ground settlement data are also of interest but are beyond the scope of this paper [see Yee et al. (2011) for data and analysis].

Following this introduction, a brief review is provided of previous studies on NL site response at vertical array sites. Then, there is a description of the geotechnical characterization of materials from the SHA site and the recorded ground motions followed by a description of equivalent-linear (EQL) and NL ground response analyses and their ability to replicate the observed near-surface recordings.

Previous Data-Model Comparisons for Nonlinear Site Response

It is important to place the value of this case history in context by comparing it to previously available case studies for NL site

[1]Assistant Professor, KEPCO International Nuclear Graduate School, Ulsan 689-882, South Korea (corresponding author). E-mail: eric.yee@kings.ac.kr

[2]Professor and Chair, Civil and Environmental Engineering Dept., Univ. of California, Los Angeles, CA 90095. E-mail: jstewart@seas.ucla.edu

[3]Professor, Tokyo Institute of Technology, Tokyo 152-8550, Japan. E-mail: kohji@o.cc.titech.ac.jp

Note. This manuscript was submitted on February 20, 2012; approved on January 25, 2013; published online on January 29, 2013. Discussion period open until March 1, 2014; separate discussions must be submitted for individual papers. This paper is part of the ***Journal of Geotechnical and Geoenvironmental Engineering***, Vol. 139, No. 10, October 1, 2013. ©ASCE, ISSN 1090-0241/2013/10-1789–1801/$25.00.

response. Stewart and Kwok (2008) led a multi-investigator project developing parameter selection and code usage protocols for NL ground response analysis. The codes/protocols were tested against the best available vertical array data not involving soil liquefaction (because the codes are for total stress analysis). The arrays utilized were a series of stiff soil sites in Japan (Kiknet), the Lotung array in Taiwan (soft silts), the La Cienega array in California (soft clay), and the Turkey Flat array in California (shallow, stiff soil). At the Turkey Flat site (Kwok et al. 2008), peak velocities from the 2004 $M_w = 6.0$ Parkfield earthquake were in the range of $7-8$ cm/s, and calculated peak ground strains were as large as 10^{-2}%. Predicted and observed acceleration histories at the surface and at intermediate depth were consistent.

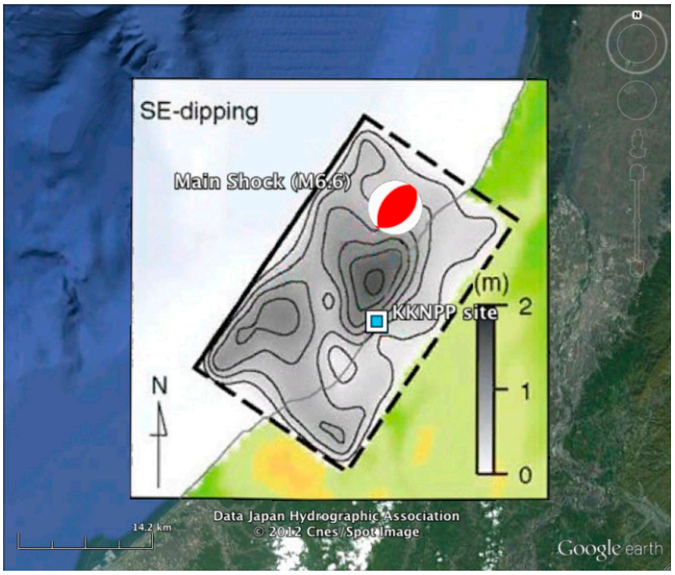

Fig. 1. Map of Kashiwazaki area showing location of KKNPP site relative to fault rupture plane by Miyake et al. (2010); shading on fault plane indicates slip in meters, © Astrium Services/Spot Image distribution

At the other sites considered by Stewart and Kwok (2008), peak velocities were 11–18 (La Cienega), 5–6 (Kiknet), and $17-31$ cm/s (Lotung). Ground strains from these other sites were of the same order as those at Turkey Flat (slightly larger at Lotung). The level of strain is important, because one of the key attributes of the parameter selection protocols is the manner by which soil backbone curves are extended from the small-strain range where dynamic soil testing is reliable (strains < 0.5%) to relatively large strains associated with the shear strength (1% or more). This is of considerable practical significance, because it is for these large-strain problems that NL ground response analysis procedures are selected for use in practice in lieu of simpler EQL methods. The SHA site provides the first example of highly NL soil behavior not involving liquefiable soils in which the induced ground strains are well in excess of 0.1%.

Tsai and Hashash (2009) used some of the same vertical array data as Stewart and Kwok (2008) in a neural network–based inverse analysis of vertical arrays to extract soil properties. Their analyses were not constrained by model-based assumptions of soil behavior and hence hold the potential to provide new insights into in situ soil behavior. However, the approach does have the potential to map modeling errors unrelated to soil behavior (e.g., lack of one-dimensional response) into inverted soil properties. The approach was applied to the Lotung and La Cienega arrays. Shear wave velocity models were slightly adjusted from data in the learning process and stress-strain loops were extracted. Modulus reduction and damping curves were then computed from the loops, which demonstrate stronger nonlinearity than laboratory-based curves (lower modulus reduction, higher damping). The observation of higher damping is also in agreement with system identification results obtained from Lotung data by Elgamal et al. (2001). The damping increases from vertical array analyses seemed to affect

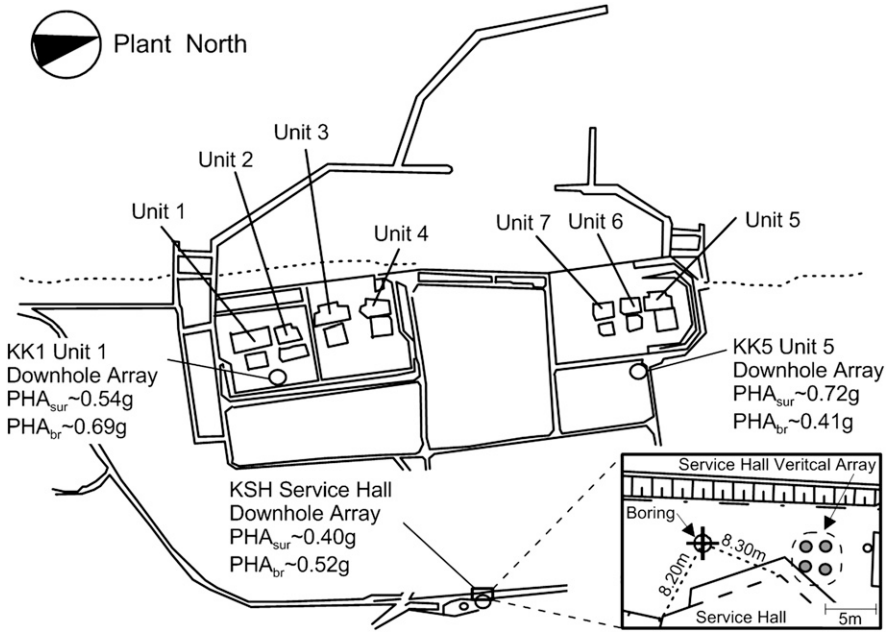

Fig. 2. Map of KKNPP showing locations of downhole arrays and geometric mean peak accelerations from 2007 Niigata-ken Chuetsu-oki earthquake; peak accelerations are shown for surface (sur) and bedrock (br) conditions; the data shown in Fig. 2 for instruments other than the SHA are taken from Tokimatsu (2008) and Tokyo Electric Power Company (2007)

J. Geotech. Geoenviron. Eng. 2013.139:1789-1801.

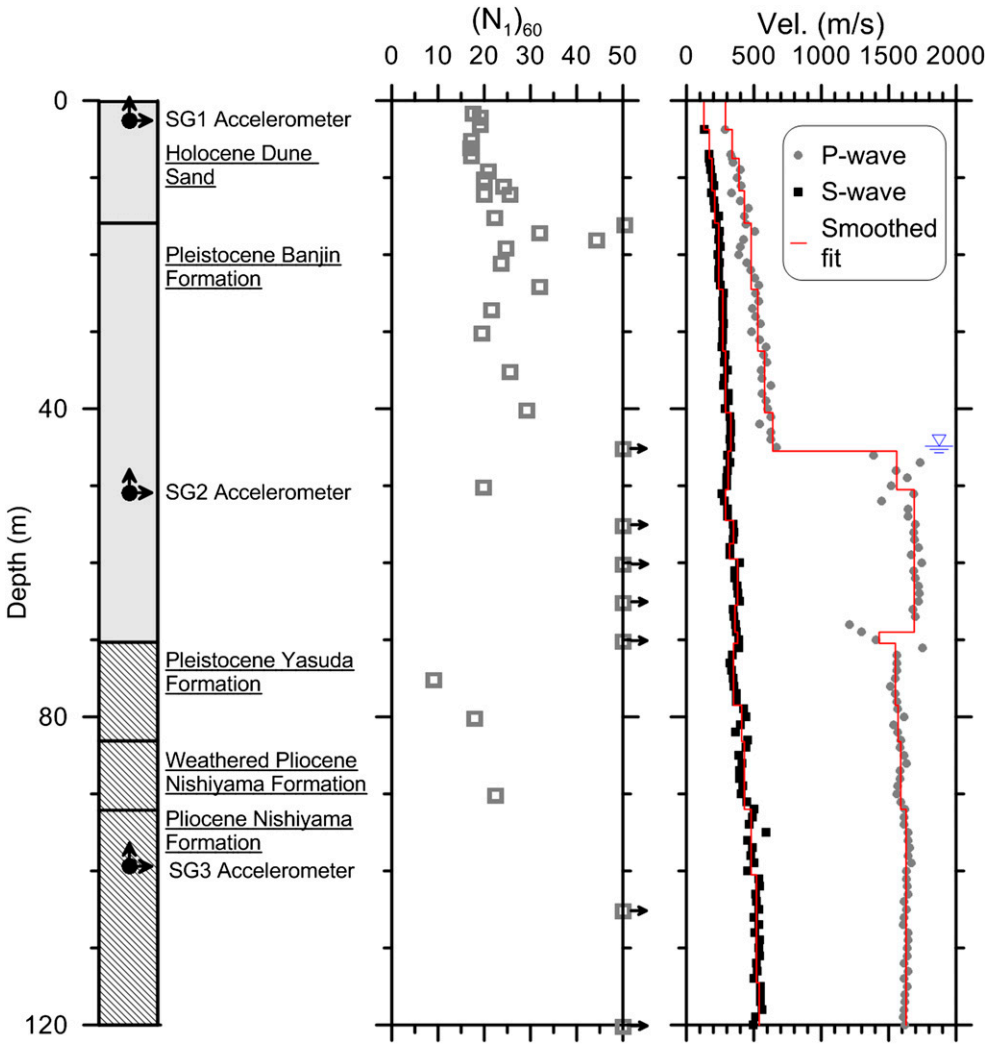

Fig. 3. Geologic log at SHA site including instrument locations and results of penetration and suspension logging geophysical testing

the small-strain damping (D_{min}) but not the overall shape of the damping-strain relationship.

Thompson et al. (2012) examined weak motion data from a large number of sites in the Kiknet vertical array network in Japan to investigate event-to-event consistency in site transfer functions (surface/downhole) and the degree to which those transfer functions are compatible with theoretical models for one-dimensional vertical shear wave propagation (SH1D). Both small and large event-to-event variability in weak motion amplification was observed for different sites; the implication of large variability for a given site is that any particular set of recordings is unlikely to represent the average site response and relatively complex event-specific attributes (such as ray path direction) are likely affecting the recordings. Of the 100 sites considered, only 16 had good fits to the SH1D model, although an unknown number of the misfits may be simply associated with modest errors in the shear wave velocity profile. Nonetheless, large misfits indicate a clearly more complex site response than SH1D. Sites such as those would not be good candidates for calculating one-dimensional NL site response for comparison with observation. For this reason, relatively weak motion aftershock data are evaluated for the SHA site to examine event-to-event variability and the consistency of observed response to SH1D predictions.

Site Characterization

A site exploration program was undertaken for the Service Hall site (SHA) at the KKNPP site that included review of prior investigations, the drilling of a borehole including standard penetration testing (SPT) with energy measurements, and suspension logging of seismic velocities. The results of this work are described in the following. This field exploration work was performed in October 2009 under contract with Tokyo Soil Research.

Results of Geotechnical Exploration

The location of the borehole drilled at the SHA site is shown in the inset of Fig. 2. The borehole was drilled using rotary wash procedures with a hole diameter of 116 mm (upper 20 m) and 86 mm (20 m to maximum depth explored of 120 m). As shown in Fig. 3, the surface geology consists of the Holocene Arahama sand dune formation (medium to fine, poorly graded sand), which overlies the Pleistocene Banjin formation (medium to fine, poorly graded sand), the Pleistocene Yasuda formation (cohesive mudstone), and the Pliocene Nishiyama formation (mudstone). Similar soil layering has been obtained in boreholes by others in the vicinity of the site (Tokyo Soil Research 2009).

J. Geotech. Geoenviron. Eng. 2013.139:1789-1801.

The SPT sampling was performed with an automatic trip-release safety hammer with a mass of 63.5 kg dropping 75 cm. Additional relatively undisturbed samples were obtained by pushing a triple-barrel pitcher sampler (similar to a Shelby tube) with an outer diameter of 76 mm and an inner diameter of approximately 74 mm. Materials from SPT samples were used for classification purposes only, whereas specimens from the pitcher sampler were used for dynamic testing. For SPT sampling, the percentage of the total theoretical energy delivered to the split-spoon sampler, or energy ratio, was measured using procedures in ASTM D6066–98 (ASTM 2000a) and ASTM D1586 (ASTM 2000b; Abou-Matar and Goble 1997). Refusal was set at 60 blows. As described further in Yee et al. (2011), energy ratios range from 84 to 94% (average of 87%) with no clear depth dependence. Energy-corrected blow counts were then calculated as

$$N_{60} = N \times \frac{ER}{60} \tag{1}$$

Overburden corrections were then applied as

$$(N_1)_{60} = N_{60} \times \left(\frac{p_a}{\sigma_v'}\right)^m \tag{2}$$

where m = function of relative density per Boulanger (2003); p_a = 101.3 kPa; and σ_v' = effective vertical stress at the sample depth (approximated as the total stress above the water table, which neglects matric suction). The resulting energy- and overburden-corrected blow counts generally range from 15 to 30 in the sandy materials and are shown in Fig. 3. No clean sand corrections are applied, because fines contents are low (< 5%).

Suspension logging was performed in our borehole to measure P and S wave velocities at 1-m intervals (Nigbor and Imai 1994). Resulting interval velocities are shown in Fig. 3. The P wave profile indicates a groundwater depth of about 45 m.

Laboratory Testing

Laboratory testing was performed to evaluate index properties, modulus reduction and damping behavior, shear strength, relative density, and cyclic volume change. Index properties, shear strength, and modulus reduction and damping behavior are described here; other properties are not utilized in the present paper but are provided in Yee et al. (2011).

Soil materials recovered from the SPT split spoon sampler were combined to form bulk samples for index tests including the grain-size distribution, Atterberg limits, and maximum and minimum unit weight. One bulk sample was prepared from sandy materials (from the Holocene and Pleistocene materials in the upper 70 m), whereas SPT samples from two relatively cohesive materials (Pleistocene mudstone from 70 to 83 m and Pliocene mudstone from 83 to 120 m) were tested separately. Results of these index tests are given in Table 1. The Holocene and Pleistocene sands are classified as poorly graded sands (SP) using the unified soil classification system with a fines content of 4.1%. The two cohesive Pleistocene samples had liquid limits of 65–69 and plasticity indexes of 22–33. The cohesive Pliocene sample had a liquid limit of 69 and a plasticity index of 22.

Soil specimens were carefully extracted from the sample tubes, trimmed, and reconsolidated for monotonic and cyclic shear testing. Because the specimens are unsaturated, no B-value measurements were made, and volume change was allowed during shear. Soil specimens were found to have sufficient cementation/cohesion to maintain their integrity upon extraction.

Consolidated-drained triaxial compression tests were performed in the Tokyo Soil Research Laboratory after consolidating three specimens from each tube to isotropic stresses of $0.5\,\sigma_v$, $1.0\,\sigma_v$, and $2.0\,\sigma_v$, where σ_v is the in situ total stress. Table 1 summarizes the test results, which indicate drained friction angles of 36–39° (average of 37.6°) for the confining pressures considered. These results are comparable to estimates from ϕ'-blow count correlations by Hatanaka and Uchida (1996), which are 35 and 41° for $(N_1)_{60}$ = 15 and 30, respectively.

Using the same triple-barrel pitcher samples from the four sample depths, additional specimens were prepared for resonant column/torsional shear (RCTS) testing in the Tokyo Soil Research Laboratory. These specimens were isotropically consolidated to in situ stresses prior to cyclic testing. Each individual sample was subjected to a series of 10 cycles at 12–13 strain amplitudes. The small-strain shear modulus (G_{max}) and material damping (D_{min}) were taken from the resonant column tests per ASTM D4015 (ASTM 2000c). At each respective strain amplitude from the torsional shear tests, the secant modulus (G) and material damping (D) were evaluated at the fifth and tenth cycles per Japanese Standard JGS 0543–2000 [Japanese Geotechnical Society (JGS) 2000] (similar to ASTM D4015). Significant changes were not observed in G and D between cycles. Fig. 4 plots the modulus reduction (G/G_{max}) and damping curves for the fifth loading cycle. The pseudoreference strains from these tests, γ_r, which is the shear strain at which $G/G_{max} = 0.5$, are listed in Table 1.

Ground Motion Data from Service Hall Array

Accelerometers at the KKNPP are owned and maintained by the Tokyo Electric Power Company. These data include acceleration recordings for the main shock and two subsequent aftershocks, named, L and S, with their epicentral and hypocentral information listed in Table 2. The SHA data were unprocessed and had baseline drift. The data were processed using procedures described by Boore (2005) and Boore and Bommer (2005) and rotated into the directions normal and parallel to the fault strike (denoted FN and FP). The FN/FP rotation was applied, because near-fault ground motions are

Table 1. Summary of Soil Index Tests, Triaxial Compression Shear Strength Tests, and Resonant Column-Torsional Shear Tests for Dynamic Soil Properties

Sample depth (m)	σ_c (kPa)	γ_{dry} (kN/m^3)	w (%)	LL	PI	Triaxial ϕ (°)	Resonant column/torsional shear		
							G_{max} (MPa)	D_{min} (%)	γ_r (%)
4–5^P	81	14.95	19.9	—	NP	39.4	50	1.3	0.057
8–9^P	153	14.23	15.0	—	NP	36.4	74	0.9	0.1
14–15^P	256	14.42	23.3	—	NP	38.7	88	1.7	0.15
20–21^P	361	14.18	11.9	—	NP	35.9	112	0.8	0.163
Bulk (sand)^S	—	—	16.6	—	NP	—	—	—	—
75.15^S	—	—	—	69	33	—	—	—	—
80.15^S	—	—	—	65	22	—	—	—	—
90.15^S	—	—	—	69	22	—	—	—	—

Note: LL = liquid limit; P = pitcher sample; PI = plastic limit; S = SPT samples.

J. Geotech. Geoenviron. Eng. 2013.139:1789-1801.

often characterized by stronger shaking in the FN direction (Watson-Lamprey and Boore 2007; Shahi and Baker 2011), which is important to consider in NL site response analysis. As described in Yee et al. (2011), high-pass corner frequencies ranging from 0.03 to 0.10 Hz were used in the processing.

Fig. 5 shows the main shock, 5% damped, pseudoacceleration response spectra for each instrument in the FN and FP directions. For each component, the spectra are similar at depths of 99.4 and 250 m (both in bedrock). As the waves travel upwards through the soil column, low-period ($T < \sim 0.6$ s) horizontal components are reduced and longer-period horizontal components are progressively amplified as shown in the spectra at 50.8 and 2.4 m, with the maximum amplification appearing to occur near 2.0 s. Comparison of the FN and FP bedrock response spectra shows larger accelerations in the FN direction, particularly at short period ($< \sim 0.2$ s) and near 3.0 s. The FN bedrock spectral peak near 3.0 s period could be a forward directivity pulse, because it lies in the range of previously observed pulse periods for shallow crustal earthquakes with comparable magnitudes ($\sim 1.3-4.0$ s, with median of 2.2 s; Shahi and Baker 2011).

Fig. 6 shows surface-to-rock (SR) transfer functions of horizontal components of the ground motions from 2.4 m normalized by those at 99.4 m depth as well as horizontal-to-vertical (H/V) spectral ratios of the surface (2.4-m) recordings. Transfer functions were computed from power spectral density functions and time-domain smoothing procedures with an effective bandwidth of 0.195 Hz using procedures described by Mikami et al. (2008). The SR transfer functions exhibit relatively similar shapes for the main shock and aftershock events. The lowest frequency peaks (indicating the apparent first-mode site frequency) from the SR transfer functions are given in Table 3. (Fundamental peaks from analyses are also given, which are described subsequently.) These apparent site frequencies are consistently lower in the FN direction relative to the FP direction, which may be because of complexities in the geologic structure. In both directions, the fundamental mode frequency decreases in the main shock relative to the aftershocks (FN: 0.83 Hz in aftershocks is reduced to 0.76 Hz; FP: 1.05 Hz is reduced to 0.95 Hz). The H/V spectral ratios are also reasonably consistent between events and indicate similar site periods as those of the SR transfer functions, as

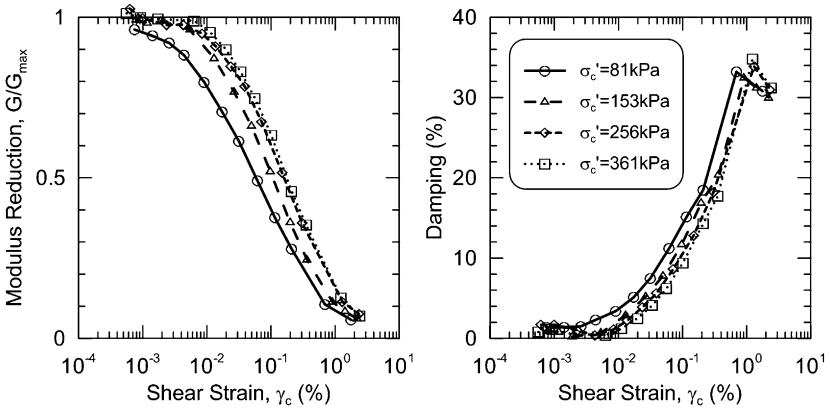

Fig. 4. Modulus reduction and damping curves from resonant column and torsional shear tests performed on specimens from four samples

Table 2. Ground Motions Used for This Study

Event	Magnitude M_w	Latitude	Longitude	Depth (km)	Distance				PGA (g)
					R_{rup} (km)	R_{jb} (km)	R_{epi} (km)	R_{hyp} (km)	
Main shock	6.6	37.53	138.45	9	16	0	—	—	0.40
Aftershock L	5.7	37.50	138.47	15	—	—	15	21	0.18
Aftershock S	4.4	37.51	138.63	20	—	—	9	22	0.04

Note: PGA = peak ground acceleration

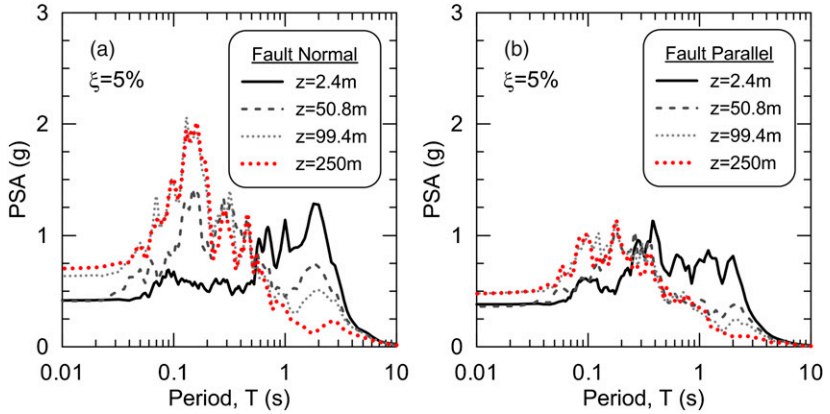

Fig. 5. Pseudoacceleration response spectra for the two horizontal components of recorded main shock ground motions at SHA site

J. Geotech. Geoenviron. Eng. 2013.139:1789-1801.

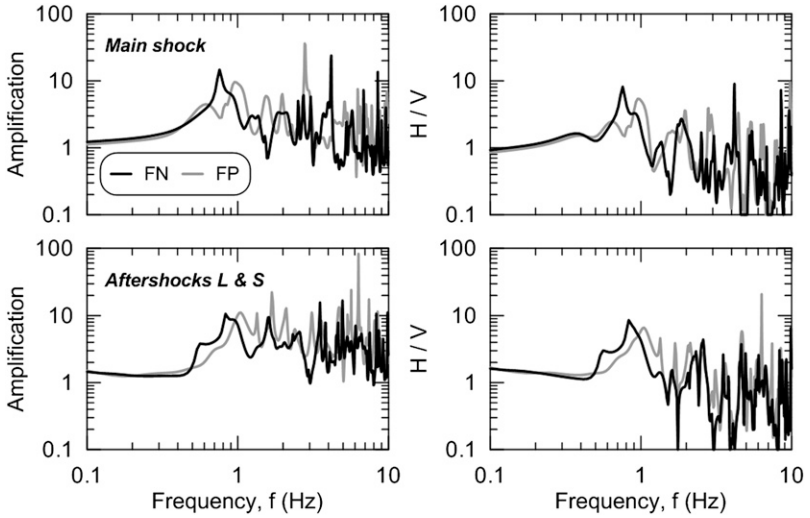

Fig. 6. Surface-to-rock (2.4-m/99.4-m) transfer functions and surface (2.4-m) H/V spectral ratios for main shock and geometric mean of aftershock recordings

Table 3. Apparent Fundamental-Mode Site Frequencies Observed from Arrays and Predicted from One-Dimensional Analysis

		Surface-to-rock transfer function		Horizontal-to-vertical peak	
Direction	Analytical (elastic) (Hz)	Main shock (Hz)	After shocks (Hz)	Main shock (Hz)	After shocks (Hz)
FN	0.72	0.76	0.83	0.76	0.83
FP	0.72	0.95	1.05	0.95	1.05

shown in Table 3. The general similarity of the SR transfer functions and H/V spectral ratios from event-to-event indicates repeatable site response, aside from the effects of nonlinearity on the resonant frequency.

Initial Ground Response Analysis of Aftershock and Main Shock Motions

Ground response analyses are used to predict one-dimensional shear wave propagation through the soil column at the SHA site. These analyses are performed using an EQL method in which the wave equation is solved in the frequency domain (Kramer 1996) and a NL method in which the soil column is represented as a multiple-degree-of-freedom system whose response to a base input motion is solved in the time domain using numerical integration. For SHA, the input motion is taken as the corrected ground motion recording within bedrock at a depth of 99.4 m. As recommended by Kwok et al. (2007), the recorded motions are used as-recorded (within condition) with a rigid base assumed below 99.4 m. Subsequent sections describe the soil properties used for these analyses (small-strain modulus and NL modulus and damping relations). Both one-dimensional EQL and NL ground response analyses are performed in *DeepSoil 4.0* (Hashash et al. 2011).

Dynamic Soil Properties for Analysis

As shown in Fig. 3, the initial shear wave velocity profile used for analysis is smoothed relative to the interval velocities from suspension logging. At a depth of about 50 m—just below the water table—there is a slight dip in the velocity profile that impacts the analysis results, as described later. Surrounding materials have shear wave velocities above 300 m/s, whereas at 50 m, shear wave velocities are about 270 m/s. Mass densities are taken from measured moist unit weights, which were approximately 16 kN/m^3 to a depth of 4 m and 17.75 kN/m^3 from 4 to 45 m. A saturated unit weight of 20.8 kN/m^3 was used from 45 to 70 m. Maximum shear modulus was computed from shear wave velocity and mass density as $G_{max} = V_s^2\rho$.

The NL constitutive models in *DeepSoil* utilize a hyperbolic backbone curve described by

$$\tau = \frac{G_{max}\gamma}{1+\beta\left(\frac{\gamma}{\gamma_r}\right)^{\alpha}} \tag{3a}$$

where γ = shear strain; γ_r = pseudoreference strain; and β and α = fitting coefficients generally taken as $\beta = 1.0$ and $\alpha \sim 0.92$ (Darendeli 2001; Zhang et al. 2005). The representation of the backbone curve as shown in Eq. (3*a*) is equivalent to taking the modulus reduction curve as

$$\frac{G}{G_{max}} = \frac{1}{1+\beta\left(\frac{\gamma}{\gamma_r}\right)^{\alpha}} \tag{3b}$$

This hyperbolic model is adopted for the backbone curve with $\beta = 1.0$. Values for parameter α are adjusted to fit the curvature of the laboratory modulus reduction curves, as described further by Yee et al. (2011). Within this framework, the only required parameters for a given depth in the soil column are G_{max} and pseudoreference strain γ_r. The parameter γ_r can be evaluated from cyclic test data (or empirical models calibrated from test data), which describe the backbone curve at small strains ($\gamma < \sim 0.3-0.5\%$). However, the hyperbolic model breaks down at large strains, where it typically produces stress estimates biased relative to the shear strength. In this section, first-order estimates of γ_r are made using available test data and models, which can be used for preliminary ground response analyses. Problematic depth intervals for which large strains develop are identified subsequently.

The RCTS test data described previously provides measurements of γ_r at the sample depths of 4, 8, 14, and 20 m, with the results in

J. Geotech. Geoenviron. Eng. 2013.139:1789-1801.

Table 1. Fig. 7 shows the pseudoreference strains from RCTS tests performed in this study and for a neighboring site compared with predictions from empirical models by Menq (2003) for sands and Darendeli (2001) for general soil types. The values of γ_r for the SHA site exceed Menq (2003) and Darendeli (2001) model predictions. The approximate variability of data around the Menq model is shown for an overburden pressure of 50.7 kPa (0.5 atm) in Fig. 7 (Menq 2003). The SHA results lie near the upper bound of the range provided by Menq (2003). A power law fit to measured pseudoreference strains was derived as

$$\gamma_r = \gamma_{r,1}\left(\frac{\sigma_0'}{p_a}\right)^n \tag{4}$$

where σ_0' = mean effective confining pressure (same as cell pressure in RCTS tests); n is taken from Menq (2003) as 0.4345; and $\gamma_{r,1}$ = regression coefficient [0.0904 ± 0.0565% for present work (range indicates 95% confidence interval), 0.0684% for sands (Menq 2003), and 0.0352% for sands (Darendeli 2001)]. The resulting fits are shown in Fig. 7.

Eq. (4) was used to estimate pseudoreference strains through most of the sand column above the water table. Below the groundwater table, where test data are not available and matric suction is zero, the Menq (2003) model is likely more accurate than the projection from Eq. (4). Accordingly, a transition is made in the γ_r used for analysis from the projected value at the deepest sample (20 m) to the Menq estimate at the base of the sand column (70 m). The Darendeli (2001) model was used to generate modulus reduction and damping curves for the relatively plastic soil and rock materials below 70 m.

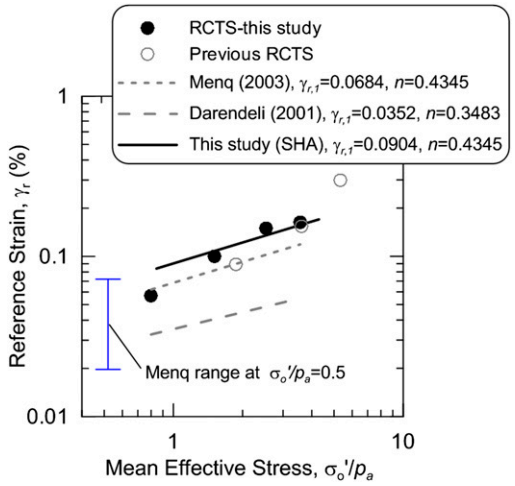

Fig. 7. Variation of pseudoreference strain with mean confining pressure from RCTS tests (this study), previous RCTS tests (neighboring site), and model predictions

Fig. 8 compares our material-specific model to RCTS test data for the sample at 20 m. Also included are the modulus reduction curves from the Darendeli (2001) and Menq (2003) models, which are plotted to the approximate strain limit of the data set used in their derivation (about $\gamma_c = 0.5\%$). The damping models are good for $D_{\min}$, so the misfit is associated with the component of the material damping model above the minimum value (i.e., $D - D_{\min}$). In the Darendeli (2001) and Menq (2003) models, the equations for $D - D_{\min}$ depend on the shape of the modulus reduction curve (as required by Masing's rules). The Darendeli (2001) and Menq (2003) model predictions use their respective modulus reduction curves. The $D - D_{\min}$ component of the Menq (2003) model was utilized with two modifications (1) use the modulus reduction curves from this study in the $D - D_{\min}$ equations and (2) increase the D above $D_{\min}$ by 40% to achieve a reasonable match to RCTS data.

Ground Response Analysis Using Aftershock Data

The analysis began by using data from aftershocks L and S to gain insight into the degree to which one-dimensional analysis can capture the site response without the complications of highly NL soil behavior affecting the interpretation. The EQL and NL methods are used with the previously mentioned soil properties and input motions with essentially identical results, so only EQL results are shown here. The ratio of effective to peak shear strains for soil property iteration were evaluated as a function of magnitude as $(M-1)/10$, which is the recommendation of Idriss and Sun (1992).

Fig. 9 shows predicted and observed SR geometric mean transfer functions for the aftershocks, and Table 3 lists observed and computed resonant frequencies. Note that the predicted transfer function provides a reasonable match to the resonant frequencies of the observed transfer functions but overpredicts the amplification at resonant frequencies. Although the data are clearly too limited to establish statistically significant empirical trends for small-strain site response, nonetheless these results are encouraging regarding the suitability of SH1D analysis for capturing site response at the SHA site [following the aforementioned logic of Thompson et al. (2012)].

Although not shown here for brevity, strain levels for the aftershocks, while relatively small (aftershock S: $\gamma_{max} = 0.01-0.02\%$;

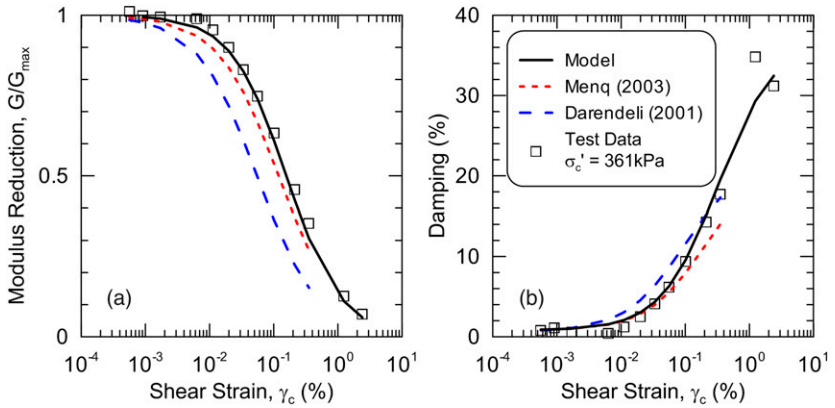

Fig. 8. Comparison of the Darendeli (2001) and Menq (2003) (a) modulus reduction and (b) damping curve models to sample test data from 20 m deep; resultant modulus reduction and damping curves are labeled Model

J. Geotech. Geoenviron. Eng. 2013.139:1789-1801.

aftershock L: $\gamma_{max} = 0.09-0.12\%$), are large enough that some modulus reduction effects are expected. As shown in Fig. 10, model-data comparisons are favorable at a depth of 50.8 m but show some overprediction of motions at 2.4 m. The overprediction of shallow motions suggests that damping ratios are underestimated from laboratory tests, which is generally consistent with previous findings by Tsai and Hashash (2009) and Elgamal et al. (2001). Accordingly, ground response analyses were repeated with small-strain damping levels in soil increased to $D_{min} = 2$ and 5% (from approximately 1% in the original models). Fig. 10 shows that the resulting spectra better matched the recorded data (especially in the FN direction and for the accelerometer at 2.4 m), although one cannot identify either value of D_{min} as the preferred choice.

Initial Ground Response Analysis Using Main Shock Recordings

Main shock ground response analyses were performed using the soil properties described previously. Several problems were encountered with these analyses. First, as shown in Fig. 11, high-frequency ground motions are significantly overestimated at 2.4 m (only slightly underestimated at 50.8 m), although this problem can be mitigated by increasing D_{min} to approximately 5%. Second, and more importantly, a spike in shear strains occurs at about 50 m that exceeds the usable limit of the backbone curves (i.e., the upper bound strains from the RCTS tests; Fig. 16). This strain localization, which occurred in NL but not EQL analyses, is caused by the dip in the V_s-profile shown in Fig. 3. It is considered unrealistic, because the maximum shear stresses mobilized in the analyses (approximately 240 kPa) are much lower than the shear strength (taken as $\sigma_v \tan\phi \approx 630$ kPa). Accordingly, the strain localization effect was removed by modification of the large-strain portions of the backbone curves, as described in the Modification of Backbone Curve to Capture Shear Strength section.

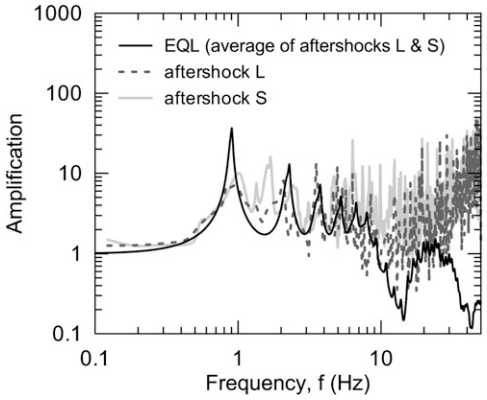

Fig. 9. Transfer functions for the main shock and two aftershocks

Modification of Backbone Curve to Capture Shear Strength

A procedure is proposed to adjust the soil backbone curve to transition toward a specified shear strength at large strains while preserving the small-strain behavior from modulus reduction curves. In this section, this procedure and its implementation in *DeepSoil* are described.

Fig. 12 schematically illustrates the proposed approach for incorporating shear strength into the backbone curve. The procedure utilizes the traditional hyperbolic backbone curve described by Eq. (3) at shear strains $\gamma < \gamma_1$, where γ_1 is a user-specified transitional shear strain. This is referred to as the first hyperbola. For $\gamma > \gamma_1$, a second hyperbola is used having an initial modulus that is the tangent modulus of the first hyperbola at γ_1 (denoted $G_{\gamma 1}$), which ensures continuity of the slope between the two hyperbolas. The second hyperbola asymptotically approaches the shear strength (τ_{ff}) at large strain. For the present site, shear strength was taken as $\sigma_v \tan(\phi)$, where ϕ was taken as 38° based on laboratory and in situ testing. The equation of the second hyperbola can be written as

$$(\tau - \tau_1) = \frac{G_{\gamma 1}\gamma'}{1 + \dfrac{\gamma'}{\gamma'_{ref}}} \tag{5}$$

where $\gamma' = \gamma - \gamma_1$; $\gamma'_{ref} = (\tau_{ff} - \tau_1)/G_{\gamma_1}$; and $\tau_1 = G_{max}\gamma_1 / [1 + (\gamma_1/\gamma_r)^{\alpha}]$. Eq. (5) matches Eq. (3*a*) except that $\beta = \alpha = 1$, the ordinates are expressed relative to a shifted set of axes with an

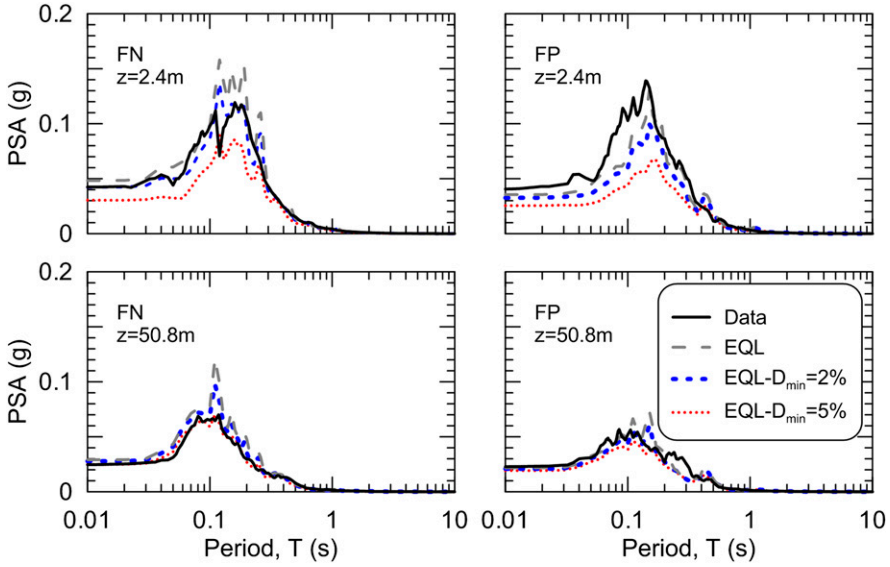

Fig. 10. Response spectra at 5% damping for aftershock S and EQL analysis results for varying levels of small-strain damping

J. Geotech. Geoenviron. Eng. 2013.139:1789-1801.

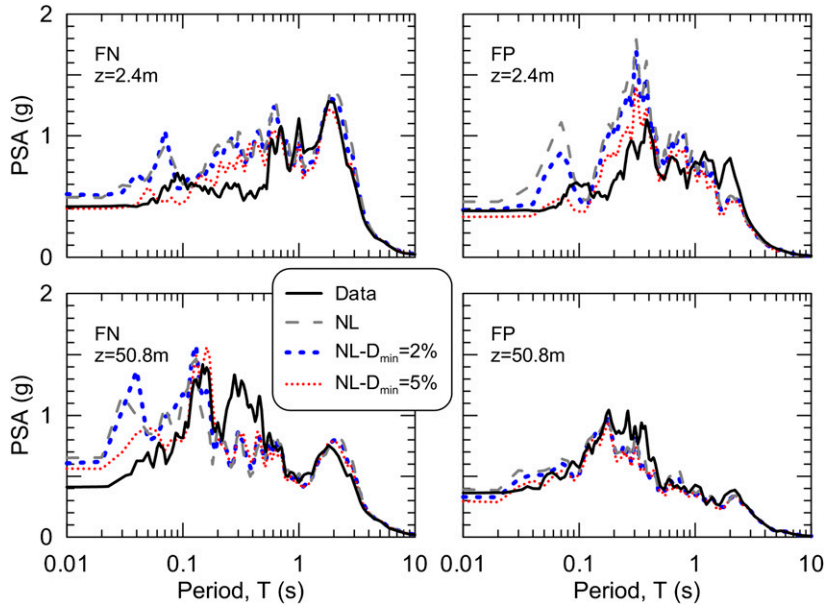

Fig. 11. Response spectra at 5% damping for main shock and NL analysis results for varying levels of small-strain damping

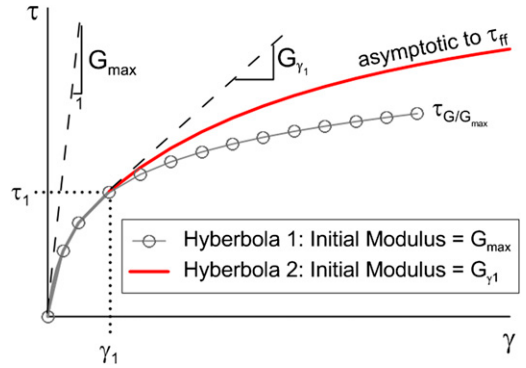

Fig. 12. Diagram for constructing shear strength–adjusted modulus reduction curves

origin at (γ_1, τ_1), and the pseudoreference strain has been replaced by an adjustment of the classical reference strain γ'_{ref} of Hardin and Drnevich (1972). The tangent shear modulus $G_{\gamma 1}$ is obtained as the derivative of Eq. (3*a*) evaluated at γ_1 as

$$\frac{G_{\gamma_1}}{G_{\max}} = \frac{1 + (1-\alpha)\left(\frac{\gamma_1}{\gamma_r}\right)^{\alpha}}{\left[1 + \left(\frac{\gamma_1}{\gamma_r}\right)^{\alpha}\right]^2} \tag{6}$$

For $\gamma > \gamma_1$, the secant modulus corresponding to points on the second hyperbola at (γ', τ') can be evaluated as the sum of τ_1 [from Eq. (3*a*)] and $\tau - \tau_1$ [from Eq. (5)] normalized by the sum of γ_1 and γ'. After manipulation to an equivalent modulus reduction relation we have,

$$\frac{G}{G_{\max}} = \frac{\dfrac{\gamma_1}{1 + (\gamma_1/\gamma_r)^{\alpha}} + \dfrac{\left(G_{\gamma_1}/G_{\max}\right)\gamma'}{1 + \left(\gamma'/\gamma'_{\text{ref}}\right)}}{\gamma} \qquad \text{for } \gamma > \gamma_1 \tag{7}$$

Two factors affect the selection of γ_1: (1) It is desirable to take γ_1 as values up to 0.3–0.5%, which is the approximate upper bound usable strain in the Darendeli (2001) and Menq (2003) models, because this provides the maximum possible range fit to empirical modulus reduction curves. (2) The shear stress at γ_1, which is $\tau_1 = G_{\max}\gamma_1/[1 + (\gamma_1/\gamma_r)^{\alpha}]$, provides practical upper bounds on the value of γ_1 that can be selected. With regard to the second factor, Fig. 13 shows that the α-parameter [Eq. (3)], which represents the curvature of the modulus reduction $(G/G_{\max})$ versus strain curve, strongly affects the values of $\tau_1/G_{\max}$ that can be achieved. As shown in Fig. 13, for values of $\alpha < 1.0$, which is the most common condition, $\tau_1/G_{\max}$ monotonically increases with γ_1. Under such conditions, it is desirable to select a value of γ_1 such that $\tau_1 \leq 0.3\,\tau_{ff}$ to achieve a reasonably smooth backbone curve shape. For larger values of $\alpha(>\sim 1.0)$, the $\tau_1/G_{\max}$ versus γ_1/γ_r relationship is peaked at $\gamma_1/\gamma_r \approx 5$–10 and τ_1 decreases for larger γ_1/γ_r. Under such conditions, it is desirable to select a value of γ_1 before the peak $(\gamma_1/\gamma_r \approx 1)$. For the current study, $\gamma_1 = 0.1\%$ was found to meet these criteria.

The program *DeepSoil* cannot accept the backbone curve functional form given previously, because it cannot be represented by a single hyperbola over the full range of strains. In this paper, we use the fitting option in *DeepSoil* in which a target curve is specified as given previously, and the best fit hyperbola is internally generated by the program. The procedure is applied for each sublayer in the site model.

A procedure similar to the one presented previously is given by Hayashi et al. (1994). The prior approach takes the backbone curve as the sum of two weighted hyperbolas, both of which utilize the true reference strain [as defined from shear strength (Hardin and Drnevich 1972)]. One of the hyperbolas is meant to apply to small strains and one to large strains. Different exponents (similar to α) are used for the two hyperbolas. Exponential weighting factors are applied to produce a smooth transition between hyperbolas. Hayashi et al. (1994) set the exponents and coefficients for the exponential weighting factors to fit laboratory data. While this is considered to be a reasonable approach to the problem, the proposed approach described previously was developed to optimize the shape of the backbone curve at small strains relative to empirical modulus reduction relations while also enabling the direct application of shear strength at large strains. The small-strain

J. Geotech. Geoenviron. Eng. 2013.139:1789-1801.

optimization is considered to be particularly important for site response problems.

Effects of Modified Backbone Curves on Analysis Results for Main Shock Motions

The new backbone curves were input into *DeepSoil*; the resultant fitted curves with no D_{min} adjustments are shown in Fig. 14. The initial model (without shear strength input) overestimates strength in shallow layers and underestimates strength in deeper layers. The damping curves have an unrealistic increase of large-strain damping (e.g., at $\gamma = 1\%$) with depth, which results from the selected relation for α, although this trend is not present at smaller strain levels ($\gamma < \sim 0.3\%$). As described in Yee et al. (2011), the parameter α affects both modulus reduction and damping behavior and was optimized to fit modulus reduction behavior, which in turn produces the large-strain damping misfit evident in Fig. 14. The damping misfit turns out to be inconsequential, as demonstrated subsequently.

Ground response analyses are performed using main shock motions, strength-adjusted backbone curves, and damping curves in soil modified to $D_{min} = 5\%$ (based on the aftershock analysis). Additional analyses at $D_{min} = 2\%$ were also performed but are not shown here for brevity [results provided in Yee et al. (2011)].

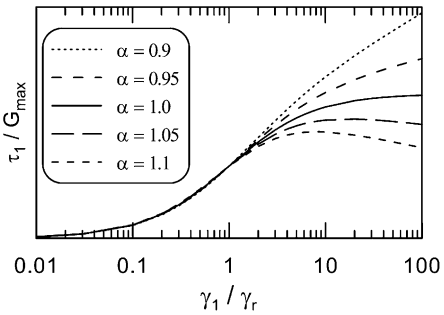

Fig. 13. Comparison of normalized backbone curve shapes (τ_1/G_{max} versus γ_1/γ_r) for different values of α

Figs. 15–17 present accelerograms and response spectra (data and simulation results), strain profiles, and maximum horizontal acceleration (MHA) profiles, respectively, for the main shock. Fig. 15 compares main shock waveforms and response spectra from the EQL and NL analyses with those from the SHA recordings at depths of 2.4 and 50.8 m. The waveform comparisons indicate general consistency of the low-frequency components that dominate the amplitude and phasing during the plotted 15- to 25-s time interval, which is the principal shear wave arrival window. The NL analyses better represent the high-frequency energy content in the initial portions of the strong shaking interval relative to EQL analysis. This is expected, because EQL analysis applies large damping throughout the shaking duration, whereas NL analyses apply damping that varies with time according to shaking intensity; such damping is generally low at the start of shaking. Based on the waveforms and pseudoacceleration response spectra (left side of figure), low-frequency features of the motions are well predicted at both depths (50.8 and 2.4 m). High-frequency features are also reasonably well predicted at both depths, although there is some overprediction at 2.4 m in the period range of 0.2–0.5 s. Also shown in Fig. 15 are the non-strength-adjusted spectra from NL analysis originally presented in Fig. 11. The comparison with strength-adjusted spectra indicates relatively little impact of the strength adjustment on spectral ordinates in this case.

The strain profiles in Fig. 16 indicate no strain localization when the strength-adjusted backbone curves are used. The computed strain levels are low enough that the unrealistic increase of large-strain damping with depth (which results from the α-model as described previously) is unlikely to affect the results. Also shown in Fig. 16 are strain profiles prior to the strength adjustment of backbone curves, which produce large strains at around 50–55 m. As shown by Yee et al. (2011), those large strains increase significantly for lower D_{min}.

Fig. 17 compares the peak accelerations within the soil column from the EQL and NL analyses to those from recordings. Results are shown for analyses before and after strength adjustment to the backbone curves. In the FN direction, peak accelerations from NL analysis are overpredicted at both depths (consistent with the findings from response spectra). This behavior is not evident in the FP direction where strains were lower. Peak accelerations from EQL analyses are closer to observed values for the FN direction.

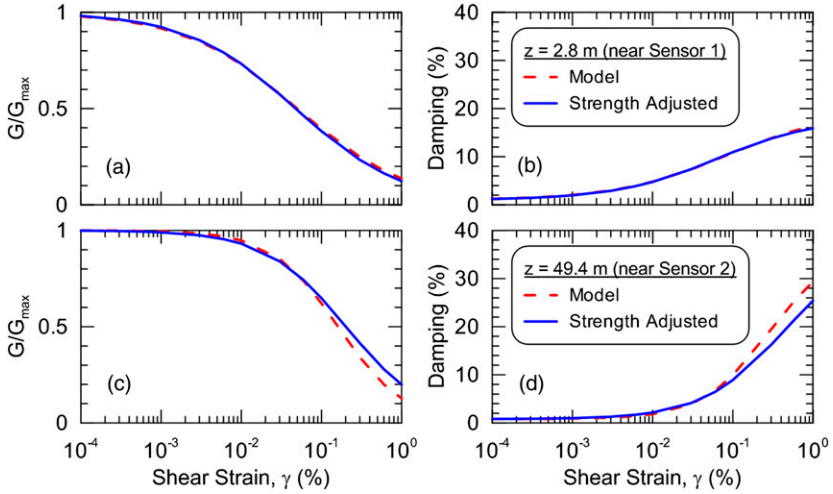

Fig. 14. Comparison of the original and strength-adjusted (a) modulus reduction and (b) damping models for the layer of soil containing the first sensor and (c) modulus reduction and (d) damping models for the layer of soil containing the second sensor

J. Geotech. Geoenviron. Eng. 2013.139:1789-1801.

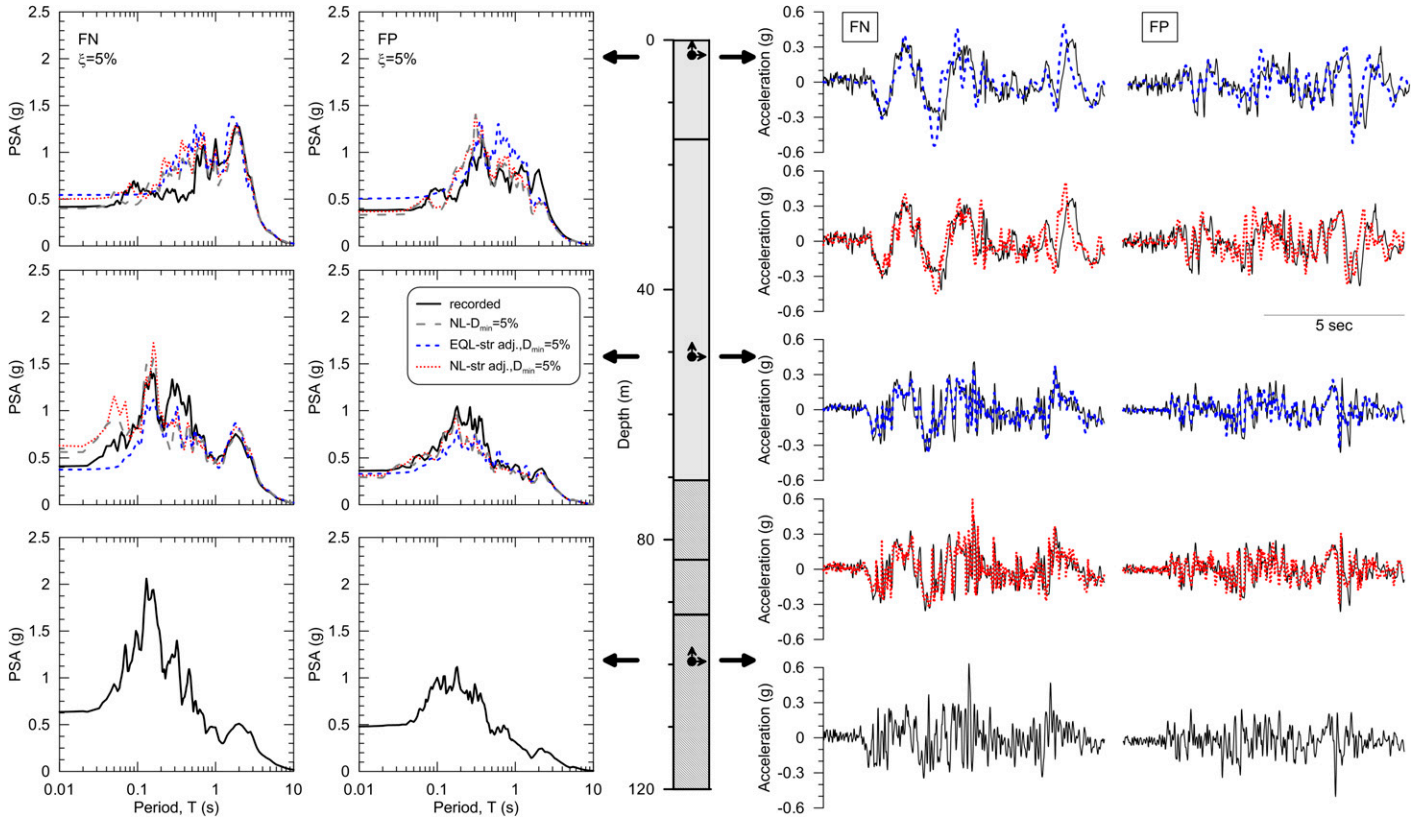

Fig. 15. Results of strength-adjusted EQL and NL ground response analyses with increased damping

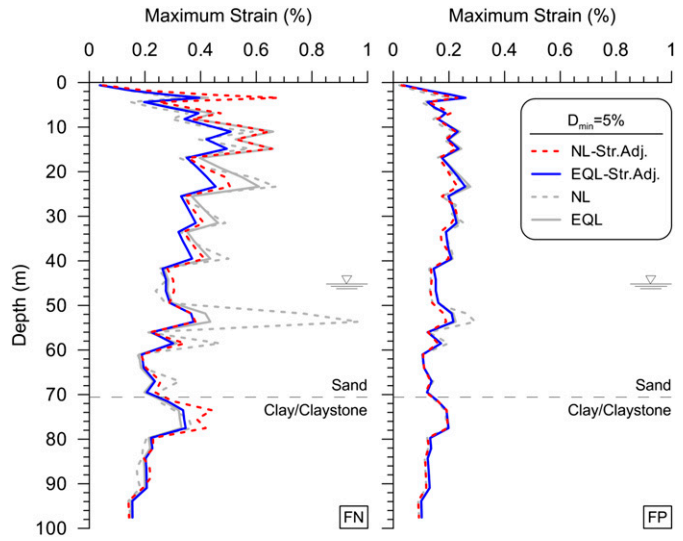

Fig. 16. Peak strain profiles from strength-adjusted EQL and NL analyses with increased damping

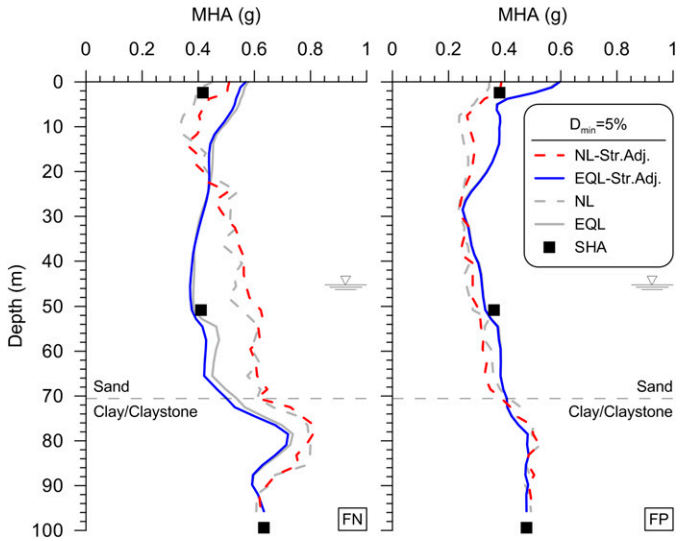

Fig. 17. Peak accelerations from increased damping on strength-adjusted NL analyses

Summary and Interpretation

The 2007 Niigata-ken Chuetsu-oki earthquake was recorded at the KKNPP site by a series of surface and downhole instruments. In this study, the focus is on the data from the SHA site where geometric mean peak accelerations at the ground surface were 0.44g. The SHA site offers a unique opportunity to validate ground response analysis codes for strong levels of shaking similar to those that would often be applied in seismic design.

A site investigation at the SHA was conducted to obtain soil samples, SPT blowcounts with energy measurements, and a velocity profile. The site profile was found to consist of about 70 m of Quaternary sands overlying Pleistocene and then Tertiary clayey bedrock materials. Triaxial compression and RCTS tests were conducted on sand specimens to measure shear strength and cyclic modulus reduction and damping curves.

The EQL and NL ground response was modeled with *DeepSoil* using the dynamic soil properties developed from field and laboratory

J. Geotech. Geoenviron. Eng. 2013.139:1789-1801.

testing and ground motion recordings from a depth of 99.4 m as input. There is some confidence in the use of one-dimensional modeling of site response for the KKNPP site as a result of repeatable surface-to-bedrock transfer functions from recorded data that are reasonably well predicted by *DeepSoil*.

Initial ground response analyses utilizing soil dynamic properties derived from RCTS tests encounter several difficulties, including overestimation of high-frequency ground response and unrealistic strain localization at a depth of 50 m from main shock ground motions in NL analyses. Increases in the small-strain material damping from laboratory-based values (near $D_{min} = 1\%$) to higher levels of $D_{min} = 2$ and 5% largely solve the problem of overprediction of high-frequency ground response. Such increases in small-strain damping are consistent with previous vertical array studies in which inferred soil damping levels exceed those from laboratory testing. A procedure to adjust backbone curves to approach the shear strength at large strains while retaining low-strain behavior from traditional modulus reduction curves was implemented to address the strain localization problem.

When the modified soil properties are implemented in ground response analysis, the strain localization problem is solved. At a small-strain damping level (in soil layers) of $D_{min} = 5\%$, the ground motion predictions from both EQL and NL analyses provide reasonably good matches to recorded response spectra from aftershock and main shock recordings at depths of 2.4 and 50 m. For the relatively strong main shock recordings, the EQL analyses overdamp the ground motions, which is evident in the time domain in the P wave window (early in the records).

Based on these results, several modifications to current practice should be considered for ground response analyses. First, when such analyses produce large-strain response, backbone curves should be adjusted to capture the shear strength at large strains. The procedure presented in this paper can be used for this purpose. It is anticipated that this correction will be needed for both EQL and NL analyses, although only the NL analysis results were more significantly affected for the present site. Second, this work and prior work by Tsai and Hashash (2009) and Elgamal et al. (2001) suggest that the soil damping derived from laboratory testing may be too low to accurately reflect in situ damping behavior. Further work will be needed to identify whether such damping increases are predictable a priori; evidence from the present analyses suggests increases in the range of 1–4% to D_{min} provide satisfactory results for the SHA site. The reasons for these damping misfits are unknown but are likely related to modeling a three-dimensional system in one dimension, which necessarily omits complexities that may introduce additional damping to the site response.

Acknowledgments

This work was supported primarily by the Pacific Earthquake Engineering Research (PEER) Center Lifelines program and by the U.S. Geological Survey external research program under contract number G11AP20039. This support is gratefully acknowledged. We also thank Akio Abe of Tokyo Soil Research Company for his efforts with the field work and RCTS laboratory testing and Pile Dynamics, Inc., for providing the equipment for SPT energy measurements. We also thank Veronica Tolnay de Hagymassy for her assistance with laboratory work at University of California, Los Angeles. Any opinions, findings, and conclusions or recommendations expressed in this material are those of the authors and do not necessarily reflect those of the PEER Center or the U.S. Geological Survey.

References

Abou-Matar, H., and Goble, G. G. (1997). "SPT dynamic analysis and measurements." *J. Geotech. Geoenviron. Eng.*, 123(10), 921–928.

ASTM. (2000a). "Standard practice for determining the normalized penetration resistance of sands for evaluation of liquefaction potential." *D6066-98*, West Conshohocken, PA.

ASTM. (2000b). "Standard test method for penetration test and split-barrel sampling of soils." *D1586*, West Conshohocken, PA.

ASTM. (2000c). "Standard test methods for modulus and damping of soils by the resonant-column method." *D4015*, West Conshohocken, PA.

Boore, D. M. (2005). "On pads and filters: Processing strong-motion data." *Bull. Seismol. Soc. Am.*, 95(2), 745–750.

Boore, D. M., and Bommer, J. J. (2005). "Processing of strong-motion accelerograms: Needs, options and consequences." *Soil. Dyn. Earthquake Eng.*, 25(2), 93–115.

Boulanger, R. W. (2003). "High overburden stress effects in liquefaction analysis." *J. Geotech. Geoenviron. Eng.*, 129(12), 1071–1082.

Cubrinovski, M., Ishihara, K., and Tanizawa, F. (1996). "Numerical simulation of the Kobe port island liquefaction." *Proc., 11th World Conf. on Earthquake Engineering*, Elsevier, Amsterdam, Netherlands, 1–8.

Darendeli, M. (2001). "Development of a new family of normalized modulus reduction and material damping curves." Ph.D. dissertation, Dept. of Civil Engineering, Univ. of Texas, Austin, TX.

DeepSoil 4.0 [Computer software]. Urbana, IL, Univ. of Illinois.

Elgamal, A., Lai, T., Yang, Z., and He, L. (2001). "Dynamic soil properties, seismic downhole arrays and applications in practice." *Proc., 4th Int. Conf. on Recent Advances in Geotechnical Earthquake Engineering and Soil Dynamics*, Univ. of Missouri-Rolla, San Diego, CA.

Hardin, B. O., and Drnevich, V. P. (1972). "Shear modulus and damping in soils." *J. Soil Mech. and Found. Div.*, 98(7), 667–692.

Hashash, Y. M. A., Groholski, D. R., Phillips, C. A., Park, D., and Musgrove, M. (2011). *Deepsoil v4.0: User manual and tutorial*, Univ. of Illinois, Urbana, IL.

Hatanaka, M., and Uchida, A. (1996). "Empirical correlation between penetration resistance and internal friction angle of sandy soils." *Soils Found.*, 36(4), 1–9.

Hayashi, H., Honda, M., Yamada, T., and Tatsuoka, F. (1994). "Modeling of nonlinear stress strain relations of sands for dynamic response analysis." *Proc., 10th Earthquake Engineering World Conf.*, Balkema, Rotterdam, Netherlands, 6819–6825.

Idriss, I. M., and Sun, J. I. (1992). *User's manual for Shake91: A computer program for conducting equivalent linear seismic response analyses of horizontally layered soil deposits*, Univ. of California, Davis, CA.

Japanese Geotechnical Society (JGS). (2000). "Method for cyclic triaxial test to determine deformation properties of geomaterials." *JGS 0542-2000*, The Japanese Geotechnical Society, Tokyo.

Kramer, S. L. (1996). *Geotechnical earthquake engineering*, Prentice Hall, Upper Saddle River, NJ.

Kwok, A. O., Stewart, J. P., and Hashash, Y. M. A. (2008). "Nonlinear ground response analysis of Turkey Flat shallow stiff soil site to strong ground motion." *Bull. Seismol. Soc. Am.*, 98(1), 331–343.

Kwok, A. O., Stewart, J. P., Hashash, Y. M. A., Matasovic, N., Pyke, R., Wang, Z., and Yang, Z. (2007). "Use of exact solutions of wave propagation problems to guide implementation of nonlinear seismic ground response analysis procedures." *J. Geotech. Geoenviron. Eng.*, 133(11), 1385–1398.

Menq, F. Y. (2003). "Dynamic properties of sandy and gravelly soils." Ph.D. dissertation, Dept. of Civil Engineering, Univ. of Texas, Austin, TX.

Mikami, A., Stewart, J. P., and Kamiyama, M. (2008). "Effects of time series analysis protocols on transfer functions calculated from earthquake accelerograms." *Soil. Dyn. Earthquake Eng.*, 28(9), 695–706.

Miyake, H., Koketsu, K., Hikima, K., Shinohara, M., and Kanazawa, T. (2010). "Source fault of the 2007 Chuetsu-oki, Japan, earthquake." *Bull. Seismol. Soc. Am.*, 100(1), 384–391.

Nigbor, R. L., and Imai, T. (1994). "The suspension ps velocity logging method." *Geophysical characterization of sites*, Richard Woods, ed., International Science, New York, 57–61.

J. Geotech. Geoenviron. Eng. 2013.139:1789-1801.

Sakai, T., Suehiro, T., Tani, T., and Sato, H. (2009). "Geotechnical performance of the Kashiwazaki-Kariwa nuclear power station caused by the 2007 Niigata ken Chuetsu-oki earthquake." *Earthquake geotechnical case histories for performance-based design*, T. Kokusho, ed., Taylor and Francis, London, 1–29.

Shahi, S. K., and Baker, J. W. (2011). "An empirically calibrated framework for including the effects of near-fault directivity in probabilistic seismic hazard analysis." *Bull. Seismol. Soc. Am.*, 101(2), 742–755.

Stewart, J. P., and Kwok, A. O. (2008). "Nonlinear seismic ground response analysis: Code usage protocols and verification against vertical array data." *Geotechnical engineering and soil dynamics IV*, D. Zeng, M. T. Manzari, and D. R. Hiltunen, eds., ASCE, Reston, VA, 1–24.

Thompson, E. M., Baise, L. G., Tanaka, Y., and Kayen, R. E. (2012). "A taxonomy of site response complexity," *Soil Dyn. Earthquake Eng.*, 41, 32–43.

Tokimatsu, K. (2008). "Geotechnical problems in the 2007 Niigata-ken Chuetsu-oki earthquake." *Geotechnical engineering and soil dynamics IV*, D. Zeng, M. T. Manzari, and D. R. Hiltunen, eds., ASCE, Reston, VA.

Tokimatsu, K., and Arai, H. (2008). "Dynamic soil behavior and rock outcrop motion back-calculated from downhole array records at Kashiwazaki-Kariwa nuclear power plant in the 2007 Niigata-ken Chuetsu-oki earthquakes." *Proc., 5th Int. Conf. on Urban Earthquake Engineering*, Center for Urban Earthquake Engineering, Tokyo Institute of Technology, Tokyo, 289–294.

Tokyo Electric Power Company. (2007). "The data analysis recorded at the Kashiwazaki Kariwa Nuclear Power Plant during the 2007 Niigata-ken Chuetsu-oki earthquake." ⟨http://www.tepco.co.jp/cc/press/betu07_j/images/070730d.pdf⟩ (Dec. 1, 2010).

Tokyo Soil Research. (2009). "Tokyo electric power Kashiwazaki-Kariwa nuclear power plant service hall geotechnical investigation." *Rep. No. 124510031*, Tokyo Soil Research, Tokyo.

Tsai, C. C., and Hashash, Y. M. A. (2009). "Learning of dynamic soil behavior from downhole arrays." *J. Geotech. Geoenviron. Eng.*, 135(6), 745–757.

Watson-Lamprey, J. A., and Boore, D. M. (2007). "Beyond Sa_{GMRotI}: Conversion to Sa_{Arb}, Sa_{SN}, and Sa_{MaxRot}." *Bull. Seismol. Soc. Am.*, 97(5), 1511–1524.

Yee, E., Stewart, J. P., and Tokimatsu, K. (2011). "Nonlinear site response and seismic compression at vertical array strongly shaken by 2007 Niigata-ken Chuetsu-oki earthquake." *Rep. No. 2011/107*, Pacific Earthquake Engineering Research Center, Univ. of California, Berkeley, CA.

Zeghal, M., Elgamal, A.-W., Tang, H. T., and Stepp, J. C. (1995). "Lotung downhole array. II: Evaluation of soil nonlinear properties." *J. Geotech. Eng.*, 121(4), 363–378.

Zhang, J., Andrus, R. D., and Juang, C. H. (2005). "Normalized shear modulus and material damping ratio relationships." *J. Geotech. Geoenviron. Eng.*, 131(4), 453–464.

J. Geotech. Geoenviron. Eng. 2013.139:1789-1801.